HHS Public Access

Author manuscript

Sci Transl Med. Author manuscript; available in PMC 2021 March 11.

Published in final edited form as:

Sci Transl Med. 2020 March 11; 12(534): . doi:10.1126/scitranslmed.aax1315.

Interdomain spacing and spatial configuration drive the potency of IgG-[L]-scFv T-cell bispecific antibodies

Brian H. Santich[1,2], **Jeong A. Park**[2], **Hoa Tran**[2], **Hong-Fen Guo**[2], **Morgan Huse**[3], **Nai-Kong V. Cheung**[2,*]

[1]Louis V. Gerstner Jr. Graduate School of Biomedical Sciences, Memorial Sloan Kettering Cancer Center, New York, NY, USA, 10065

[2]Department of Pediatrics, Memorial Sloan Kettering Cancer Center, New York, NY, USA, 10065

[3]Immunology Program, Memorial Sloan Kettering Cancer Center, New York, NY, USA, 10065

Abstract

T cell bispecific antibodies (BsAb) couple cytotoxic T lymphocytes to tumor cells, inducing their destruction. Although there are over 60 classes of BsAb in development, the relative importance of parameters such as interdomain spacing or spatial configuration are largely unknown. Here, we dissected a symmetric dual bivalent BsAb platform (IgG-[L]-scFv: anti-tumor IgG with anti-CD3 scFv fused to the light chains) to explore the importance of valency and spatial configuration for BsAb-induced T cell cytotoxicity. Our results revealed that placing tumor and T cell binding domains on the same side of a BsAb (cis configuration) elicited substantially stronger anti-tumor activity, in vitro and in vivo, compared to positioning them on opposite sides (trans configuration). Moreover, using two cis-modules in the same BsAb further improved cytotoxicity (up to 2,000-fold). Additionally, separating antigen-binding components with a single Ig domain (C_L) dramatically enhanced cytokine release and in vivo tumor responses compared to smaller (G_4S_1) or larger (C_{H1}-C_{H2}-C_{H3}) spacers. These findings provide guidelines for improving BsAb function and highlight the importance of spatial configuration and dual bivalency as development parameters.

One Sentence Summary:

T cell bispecific antibody anti-tumor function is maximized through optimal interdomain spacing and dual cis-configurations.

*Corresponding author Nai-Kong Cheung, MD PhD, Department of Pediatrics, Memorial Sloan Kettering Cancer Center, 1275 York Avenue, New York, New York, USA, 10065, Tel No. 646-888-2313, Fax No. 646-422-0452, cheungn@mskcc.org.

Author contributions: BS, MH, and NKC designed the experiments, interpreted the results and wrote the manuscript. BS, JP, HT, and HFG performed and/or analyzed the experiments.

Competing interests: BS, MH and NKC were named as inventors on US patents filed by MSKCC (Heterodimeric Tetravalency and Specificity Antibody Compositions and Uses Thereof, US 62/774,111). Anti-GD2 antibodies were licensed by MSKCC to Y-mAbs Therapeutics Inc. NKC reports receiving sponsored research grants from Y-mAbs and Abpro-Labs Inc.; holding financial interest in Y-mAbs, Abpro-Labs, and Eureka Therapeutics. NKC was also named as an inventor on patents both currently unlicensed and licensed by MSK to Y-mAbs Therapeutics, Biotec Pharmacon, or Abpro-Labs (Anti-GD2 Antibodies (h3F8), US 61/397,920; High Affinity Anti-GD2 Antibodies, US 61/801,287; Anti-CD33 Antibody Agents, 62/489,269). NKC is an advisory board member for Abpro-Labs and Eureka Therapeutics. The other authors declare they have no competing interests.

Data and materials availability: All data supporting the findings of this study are available within the paper or supplementary materials. Antibodies and their amino acid or DNA sequences can be obtained from the corresponding author.

Introduction

In recent years, bispecific antibody (BsAb) development has emerged as a promising strategy for the treatment of clotting deficiency (1) and cancer (2–4). While only two different formats have been used in FDA-approved BsAbs to date (1, 2), there are over 60 currently in preclinical and clinical development (5–7). This proliferation of different BsAb formats has generated a panoply of designs with distinct sizes, valencies, and interdomain configurations. Although studies have suggested that molecular size and tumor binding affinity can influence biodistribution (8) and cytotoxicity (9), respectively, the importance of other structural features remains largely unknown. Systematic efforts to identify the parameters that most influence in vitro and in vivo BsAb potency are critical for developing the best therapeutics to improve outcomes in the clinic.

We have previously described several highly potent T cell engaging BsAbs using the symmetric and dual bivalent IgG-[L]-scFv platform (10–13), in which a single chain variable fragment (scFv) recognizing human CD3ε (huCD3ε) is fused to the C-termini of each anti-tumor antibody light chain (Fig. 1A). While this design has consistently provided exceptionally strong in vitro and in vivo anti-tumor activity against multiple tumor antigens (ganglioside GD2(13), CD33(10), GPA33(11), and HER2(12)), the basis for its efficacy is poorly understood.

In the present study, we examined a particularly powerful GD2-specific IgG-[L]-scFv reagent and identified architectural features that explain its robust anti-tumor activity. First, we confirmed the importance of valency for improving in vitro cytotoxicity. Next, we demonstrated that separation of tumor and T cell binding domains using a single Ig domain (C_L) drastically improved in vitro cytokine secretion and in vivo anti-tumor responses compared to smaller (G_4S_1) or larger (C_{H1}-C_{H2}-C_{H3}) spacers. Finally, through systematic re-engineering of the IgG-[L]-scFv design, we showed that placing tumor and T cell binding domains on the same side of a BsAb (cis-configuration) improved cytotoxic potencies 50-fold and that uniting two such cis-modules together in one dual bivalent format increased in vitro cytotoxicity an additional 30-fold, dramatically enhancing naïve T cell responses both in vitro and in vivo. Hence, the potency of a BsAb results not only from its valency, but also from the spacing and spatial configuration of its antigen-binding domains.

Results

IgG-[L]-scFv format is substantially more potent than other common BsAb designs

We began our study by comparing the IgG-[L]-scFv format to two BsAb formats widely used for T cell redirection applications: the Bispecific T-cell engager (BiTE; same format as the FDA-approved blinatumomab) and the IgG-heterodimer (Fig. 1A and table S1). Each BsAb was engineered to recognize ganglioside GD2 (GD2) on tumor cells and human CD3ε (huCD3ε) on T cells using the variable domain sequences of humanized 3F8 (hu3F8) (14) and humanized OKT3 (huOKT3) (15), respectively. Both the BiTE and the IgG-[L]-scFv BsAb were produced using standard mammalian expression and affinity purification, while the IgG-heterodimer was made through the controlled Fab Arm Exchange (cFAE) (16) of

two distinct IgG homodimers (hu3F8 IgG and huOKT3 IgG). For each of these parental IgG molecules, one of two Fc mutations were introduced (hu3F8 with K409R or huOKT3 with F405L) to facilitate their monomerization and preferential heterodimerization under reducing conditions (Fig. 1B and table S1).

We measured the binding kinetics of each BsAb format against GD2 and huCD3ε using surface plasmon resonance (SPR) (table S2 and S3). Not surprisingly, the IgG-[L]-scFv, hereafter called 2+2 (for two anti-GD2 and two anti-huCD3ε domains), displayed higher apparent affinity for both antigens (3 nM K_D for GD2 and 6 nM for huCD3ε) when compared to both the BiTE (11 nM K_D for GD2 and 13 nM for huCD3ε) and IgG-heterodimer (15 nM K_D for GD2 and 130 nM for huCD3ε), hereafter called 1+1B and 1+1H (for one anti-GD2 and anti-huCD3ε domain), respectively. Binding to antigen-expressing cells was evaluated by flow cytometry (Fig. 1C, data file S1), detecting bound BsAb with anti-idiotypic antibodies that recognized either the anti-huCD3ε domains (to measure GD2 binding) or the anti-GD2 domains (to measure CD3 binding) of each BsAb. Here 2+2 bound GD2(+) human M14 melanoma cells much more effectively than 1+1H or 1+1B, both in terms of maximum binding and binding EC_{50}, while all three formats bound similarly to activated human T cells (huATC).

To assess the potency of each format, we performed in vitro cytotoxicity assays where the BsAb engaged huATC against M14 human melanoma cells (Fig. 1D and table S1). Strikingly, 2+2 (9 fM EC_{50}) was over 500-fold more potent than 1+1H (4 pM EC_{50}) and over 20-fold more potent than 1+1B (230 fM EC_{50}). To confirm that these differences were not specific to the hu3F8 sequence, two additional anti-GD2 sequences (GD2.2, GD2.3) were used to build both 2+2 and 1+1H formats (table S4). Both constructs recapitulated the in vitro cytotoxicity differences seen with the hu3F8-based 2+2 and 1+1H formats (857- and 1,959-fold, respectively), suggesting that the dramatically enhanced potency of 2+2 was not unique to the hu3F8 sequence. These results were also consistent with prior studies showing that a 2+2 BsAb directed against CD33 was 100-fold more cytotoxic than its 1+1H counterpart (10), indicating that this major difference in cytotoxicity was not restricted to GD2 or membrane-proximal antigens. We also prepared 1+1B formatted BsAb using the GD2.2 and GD2.3 sequences. Although only one of these (GD2.2) expressed at high enough purity (>80% monomer) to make meaningful interpretations, it too showed reduced potency compared to the analogous 2+2 (table S4). Finally, to determine if the enhanced efficacy of 2+2 resulted from unique properties of the huOKT3 sequence or epitope, we made 2+2 and 1+1H BsAb using an anti-mouse CD3ε (muCD3ε) antibody sequence (145–2C11)(17). Both formats bound muCD3ε with similar affinities (62 nM K_D for 2C11 2+2 and 95 nM) for 2C11 1+1H), which were substantially lower than what was observed with the anti-human CD3ε 2+2 and 1+1H BsAb (table S5 and fig. S1). Nevertheless, we found that the 2+2 format (0.8 pM EC_{50}) outperformed the 1+1H (9.9 pM EC_{50}), albeit to a lesser extent than we observed with the huOKT3 variants (table S4). Collectively, these results suggest that the cytotoxic advantage of 2+2 over 1+1H is at least partially due to the format of the molecule.

We next investigated whether the enhanced in vitro potency of 2+2 would translate into superior anti-tumor activity in vivo (Fig. 2, fig. S2 and S3). First, we used a xenograft mouse

model in immunodeficient IL-2rg$^{-/-}$ Rag2$^{-/-}$ BALB/c mice (DKO) (12) (Fig. 2A). DKO mice were implanted subcutaneously with human melanoma tumors (M14) and then treated intravenously with huATCs and BsAb. 2+2 elicited strong anti-tumor activity, shrinking large tumors (up to 1,000 mm^3) in all treated mice (Fig. 2B), whereas 1+1H failed to confer any benefit relative to a control BsAb (an IgG-[L]-scFv directed against an irrelevant tumor antigen).

Comparing 2+2 with 1+1B in vivo was complicated by their vastly different pharmacokinetic properties; 1+1B had a short serum half-life of ~15 min (18), compared to ~3 days for 2+2 (table S6). To circumvent this issue, we used an ex vivo “armed” T cell (EAT) xenograft model in which huATCs were pre-bound with BsAb, washed, and then injected into neuroblastoma PDX-bearing DKO mice (fig. S2A). The goal was to create chimeric antigen receptor (CAR)-like T cells that acquired their tumor-binding potential before adoptive transfer. Any differences in their subsequent anti-tumor function could then be directly related to the cytotoxic potency of the BsAb used to “arm” them. For these experiments, 2+2, 1+1B, and 1+1H preincubation protocols were optimized such that all EATs contained comparable amounts of anti-GD2 binding domains (fig. S2B). Importantly, all three BsAbs remained stably bound to huATCs at 37 °C for up to 3 days in vitro (fig. S2C), indicating that the EATs could indeed be treated as CAR-like T cells. However, in vivo, 2+2 EAT displayed robust anti-tumor activity, while 1+1H and 1+1B EAT both failed to show any benefit (fig. S2D). These results confirm the enhanced efficacy of 2+2 and demonstrate that its superiority does not arise solely from its pharmacokinetics.

Lastly, we tested each of the BsAbs in a syngeneic model using C57BL/6 mice that carried a huCD3ε transgene (huCD3ε-tg) (19). T cells in these mice co-express the huCD3ε protein along with the native murine homolog, allowing our BsAbs to engage naïve T cells directly in their natural setting (fig. S3A). Importantly, despite 2+2 having bivalency toward huCD3ε, none of the mice in our syngeneic experiments displayed overt signs of toxicity such as weight loss or piloerection. 2+2 did induce a modest reduction in white blood cells (WBCs) after the first dose (fig. S3B), however, we observed a similar drop in 1+1H and 1+1B treated mice, implying that this was not specific to bivalent T cell engagement. Consistent with the results of the xenograft models, 2+2 treated mice displayed significant ($P < 0.0001$) growth inhibition of subcutaneous GD2(+) EL.4 lymphoma tumors. Neither 1+1H nor 1+1B treated mice showed any benefit (fig. S3C), despite daily dosing of 1+1B to mimic the continuous infusion methods used clinically, indicating that the enhanced activity of the 2+2 design applied to both naïve and preactivated T cells. Taken together, the results of our in vitro data and three different animal models demonstrate that the IgG-[L]-scFv format drives substantially more robust anti-tumor responses than either BiTE or IgG-heterodimer formats.

Interdomain spacing is critical to IgG-[L]-scFv format’s anti-tumor activity

We next evaluated two additional dual bivalent BsAb formats (Fig. 3A and table S7), an IgG-[H]-scFv (2+2HC)(20) and a human IgG$_1$ based BiTE-Fc (2+2B)(6). In contrast to 2+2, which used a single Ig domain (C_L) to separate tumor and T cell binding components, 2+2HC increased the spacing to three Ig domains (C_{H1}-C_{H2}-C_{H3}) by fusing each anti-

huCD3ε scFv to the C-terminus of each anti-GD2 heavy chain. Conversely, 2+2B used a short (G_4S_1) linker between each pair of scFv's to reduce the spacing between tumor and T cell binding domains. All three BsAb bound GD2(+) human M14 melanoma cells comparably in flow cytometry assays (Fig. 3B), however, their binding to T cells was surprisingly different. 2+2B bound most effectively, displaying enhancement in both maximum binding and binding EC_{50} relative to both 2+2 and 2+2HC. 2+2HC exhibited about 10-fold greater T cell binding potency than 2+2, with comparable maximum binding. These results reveal that interdomain spacing is critical for robust T cell engagement and imply that, in contrast to the 2+2B format, 2+2 and 2+2HC may not be capable of consistent bivalent CD3 engagement.

Surprisingly, both 2+2B and 2+2HC exhibited reduced in vitro cytotoxicity compared to 2+2 (Fig. 3C and table S7), lysing tumor cells with ~2- to ~3-fold lower potency compared to 2+2 (80 fM and 140 fM EC_{50}, respectively, versus 38 fM in 2+2). To further investigate these unexpected differences in in vitro function, we performed co-culture assays (Fig. 3D, fig. S4 and S5) with naïve human T cells and GD2(+) M14 melanoma cells, using T cell activation and cytokine release as downstream readouts. 2+2 induced substantially stronger interleukin-2 (IL-2) cytokine release compared to either 2+2HC or 2+2B, in terms of both overall response and potency. 2+2 also elicited more potent upregulation of the early response surface markers CD69 and CD25 (fig. S5A), confirming that 2+2 activated T cells more effectively than 2+2B or 2+2HC. Importantly, none of the BsAb induced measurable cytokine release or T cell activation in the absence of tumor cells (fig. S5B), demonstrating that these responses were entirely antigen-dependent.

To determine the effects of interdomain spacing on in vivo tumor responses, we compared these three formats using both the conventional (Fig. 4) and the EAT (fig. S6) xenograft models. In both systems, only 2+2 elicited robust anti-tumor responses, while 2+2B and 2+2HC displayed minimal efficacy relative to untreated or unarmed controls. These results were unexpected and suggested two important points: 1) bivalency alone was insufficient to drive strong anti-tumor function, and 2) reducing interdomain spacing did not necessarily confer increased cytotoxicity. Instead, the superiority of the 2+2 design implied that optimal interdomain spacing and spatial configuration was critical for driving the most robust in vitro and in vivo anti-tumor responses.

Valency improves tumor and T cell binding of IgG-[L]-scFv format

To identify the properties of the IgG-[L]-scFv format responsible for its striking anti-tumor activity, we engineered four new IgG-[L]-scFv heterodimers (Fig. 5 and table S8), which represented all possible combinations of valency and interdomain spatial configurations. As before, heterodimers were made by first producing the necessary homodimeric parental IgG or IgG-[L]-scFv proteins containing either K409R or F405L substitutions in the Fc region. By using a combination of IgG antibody and IgG-[L]-scFv BsAb directed against GD2 or an irrelevant antigen (CD33) (10), all possible variations of the anti-GD2 IgG-[L]-scFv format were produced (Fig. 5A–B); 1+2 had one anti-GD2 domain replaced by a non-binding anti-CD33 domain (humanized M195), 2+1 had one anti-huCD3ε domain removed, and each 1+1 had one anti-GD2 domain replaced and one anti-huCD3ε domain removed, either from

the same side (cis) or from opposite sides (trans), hereafter named 1+1C and 1+1T, respectively. The purity of each preparation was confirmed using SEC-HPLC and CZE to assess size and charge, respectively (table S8).

We began our comparative analyses by determining the antigen binding affinity of all constructs by SPR (table S9 and S10). As expected, BsAb containing two GD2-binding Fabs (2+2 and 2+1) had higher apparent GD2 affinity (~3 nM K_D) than monovalent formats (1+2, 1+1T, 1+1C, 1+1H, ~30 nM K_D). Similarly, BsAb with two huCD3ε-binding scFvs (2+2 and 1+2) had higher apparent CD3 affinity (~10 nM K_D) than formats with only one (2+1, 1+1T, 1+1C, 1+1H, 70–300 nM K_D). Flow cytometric evaluation of the binding activity of each BsAb against M14 melanoma cells and huATCs was consistent with the SPR data, with bivalent BsAb exhibiting stronger binding to cell-associated antigen than their monovalent counterparts (Fig. 5C).

To assess how differences in binding to GD2 and huCD3ε might compound when both antigens were engaged simultaneously, we performed an in vitro cell-to-cell conjugate assay (Fig. 5D, fig. S7). Tumor cells and huATCs were differentially labeled with either cell trace violet (CTV) or CFSE, respectively, briefly incubated together with different concentrations of BsAb, and then fixed in formaldehyde for flow cytometric analysis. 2+2 induced T cell:tumor cell conjugates most effectively in this assay, followed by 2+1. The remaining formats (1+2, 1+1T, 1+1C, and 1+1H) exhibited markedly less activity, although all performed better than a non-targeting control BsAb. These results indicated that bivalency, especially against the tumor, improved conjugate formation, an important step towards cytotoxicity. Importantly, 1+1C and 1+1T were indistinguishable in their capacity to bind antigen or induce conjugates, which indicated that the spatial configuration of tumor and T cell binding domains did not impact conjugate formation.

Spatial configuration determines IgG-[L]-scFv function in vitro and in vivo

In vitro cytotoxicity assays targeting M14 melanoma cells revealed striking differences within the IgG-[L]-scFv panel (Fig. 6A and table S8). 2+2 induced the strongest anti-tumor cytotoxicity (26 fM EC_{50}), followed by 2+1 (240 fM EC_{50}) and 1+2 (773 fM EC_{50}), which were ~9 fold and ~30 fold less effective, respectively. Surprisingly, 1+1C (780 fM EC_{50}) was essentially equipotent to 1+2, despite having markedly less binding activity to huCD3ε. The potency of 1+1T (37 pM EC_{50}), by contrast, was similar to that of 1+1H (20 pM EC_{50}), which was ~50 fold worse than 1+2 and 1+1C, and over 1,000-fold worse than 2+2. To confirm that these results were not GD2-specific, we performed reciprocal cytotoxicity experiments targeting CD33. Because an anti-CD33 Fab was used as the control arm for the anti-GD2 IgG-[L]-scFv panel, only two additional heterodimers needed to be made for these studies – CD33 2+1 and CD33 1+1H – whereas 1+2, 1+1T, and 1+1C from the GD2 panel could be directly applied. CD33 2+2 (0.9 pM EC_{50}) was the most potent design, followed by CD33 2+1 (4.5 pM EC_{50}), 1+2 (6.0 pM EC_{50}), CD33 1+1C (aka GD2 1+1T, 11.5 pM EC_{50}), CD33 1+1H (134 pM EC_{50}), and finally CD33 1+1T (aka GD2 1+1C, 500 pM EC_{50}) (table S11). This confirmed that the rank order of cytotoxic activity exhibited by the various IgG-[L]-scFv variants was a generalizable property of format architecture, and not specific to the tumor antigen.

To explore how differences in valency and spatial configuration impacted naïve T cell activation, we compared the panel of IgG-[L]-scFv using an in vitro co-culture assay (Fig. 6B–F, fig. S4, S8). Once more, IL-2 secretion revealed major differences between the different BsAb variants. 2+2 elicited substantially stronger IL-2 secretion than all other BsAbs, displaying nearly 100-fold higher potency than the next most stimulatory variant (Fig. 6B). 2+1, 1+2, and 1+1C exhibited intermediate potencies, and 1+1T and 1+1H induced weak IL-2 secretion near the lower limit of detection. T cell activation and proliferation generally followed the same rank order, although with smaller differences, and remained consistent for both CD4(+) and CD8(+) T cell subsets (Fig. 6C–F, fig. S8A–B). 2+2 displayed the highest potency, whereas 1+1T was consistently the weakest variant, indistinguishable from 1+1H and about 200-fold less stimulatory than 2+2. 2+1, 1+2, and 1+1C generally clustered together at intermediate potencies, with 2+1 displaying slightly more effective activation, followed by 1+2 and then 1+1C. As before, T cells incubated with BsAb, but without tumor cells, did not exhibit any measurable responses (fig. S8C), indicating that BsAb-mediated T cell activation was antigen-dependent.

The consistent and striking differences in efficacy between 1+1C and 1+1T suggested that the spatial configuration of antigen-binding domains was a key determinant of BsAb activity in vitro. Furthermore, whereas 2+2 displayed clear benefits over 2+1 and 1+2, neither 2+1 nor 1+2 was superior to 1+1C. Hence, the addition of antigen-binding domains improved function most effectively when it created an additional cis-module. Taken together, these data demonstrate that dual bivalency within the IgG-[L]-scFv framework enhances BsAb function by improving cell binding and presenting tumor and T cell binding domains in cis-configuration.

To determine the effects of valency and spatial configuration on in vivo tumor responses, we examined the IgG-[L]-scFv panel using both xenograft and syngeneic tumor models (Fig. 7 and fig. S9). In DKO mice bearing subcutaneous human melanoma (M14) tumors and treated with BsAb and huATCs (Fig. 7A), 2+2 again displayed the strongest anti-tumor activity (Fig. 7B). 2+1 initially elicited similar responses to 2+2, but ultimately had inferior durability, with tumors recurring quickly after treatment ended. Consistent with the in vitro functional studies, 1+2 and 1+1C both exhibited moderate anti-tumor activity, but they were noticeably worse than 2+1 and 2+2. Finally, both 1+1H and 1+T failed to show any anti-tumor efficacy relative to mice treated with control BsAb.

Results were more polarized in the syngeneic model (fig. S9A). Here, only 2+2 displayed measurable anti-tumor activity, whereas all other BsAb completely failed to inhibit tumor growth (fig. S9B). Importantly, none of the BsAb-treated mice displayed any indices of toxicity, such as weight loss or piloerection. Although all members of the IgG-[L]-scFv panel modestly increased plasma IL-6, they did so to a much lesser extent than did a positive control reagent containing a full-length OKT3 IgG antibody (21) (fig. S9C), indicating that the IgG-[L]-scFv design did not elicit measurable amounts of antigen-independent activation or cytokine release, and further demonstrating that bivalency against CD3 in the IgG-[L]-scFv design was safe and effective. Collectively, these results are consistent with our in vitro findings and confirm the importance of cis-configured tumor and T cell binding domains.

Discussion

In this study, we directly examined how the IgG-[L]-scFv design improved anti-tumor responses compared to multiple other formats targeted against both GD2 and CD33. We found that dual bivalency was crucial for function, but surprisingly not for the reasons we had initially anticipated. Although bivalency had the expected effect of enhancing binding against both tumor cells and T cells, several of our results indicated that this was of secondary importance therapeutically. For instance, although 2+2B (BiTE-Fc) and 2+2HC (IgG-[H]-scFv) exhibited similar tumor binding and superior T cell binding relative to 2+2, both failed to show anti-tumor activity in vivo. Furthermore, adding a second anti-tumor Fab (GD2 or CD33) to 1+1C (to generate 2+1) provided only a modest improvement in activity, and adding a second anti-huCD3ε scFv to 1+1C (to generate 1+2) made essentially no difference. Indeed, effective in vitro and in vivo anti-tumor activity were better correlated with two other properties: 1) the spatial orientation of tumor and T cell binding domains in a cis-configuration, and 2) their separation by a single Ig spacer (C_L). Using these two criteria, all tested formats are easily grouped into a rank order of ascending efficacy: zero cis-modules (low potency): 1+1T, 1+1H; two cis-modules with suboptimal interdomain spacing (low-moderate potency): 2+2B, 2+2HC; one cis-module with optimal interdomain spacing (moderate potency): 2+1, 1+2, 1+1C; and two cis-modules with optimal interdomain spacing (high potency): 2+2. Moreover, the beneficial effects of cis-configurations and interdomain spacing that we have observed are consistent with a recent report describing a high potency T cell BsAb containing a single cis module (Fab-Fab) (22). We conclude that, in the case of T cell BsAb, the total number of interactions matters less than the way those interactions are made.

Although most of our experiments used reagents derived from 3F8 (anti-GD2) and OKT3 (anti-huCD3), other sequences were also examined to assess the generalizability of our findings. While we were able to corroborate key observations using BsAb based on clone M195 (targeting CD33 on tumors) the functional advantage of the 2+2 format was less pronounced when we used an alternative CD3-binding clone (145–2C11, targeting murine CD3) to engage T cells. Here it is important to note that many other anti-CD3 sequences are under development in T cell BsAbs, and it is possible that some may behave differently than OKT3 within the IgG-[L]-scFv design, depending on their binding affinity and epitope. A more thorough examination of the 2+2 design with additional anti-CD3 modules would be an interesting topic for future research. Nevertheless, we feel that our findings are broadly relevant to clinical practice, in particular because OKT3 continues to be one of the most clinically used sequences in T cell BsAbs (7) and is the backbone of the only FDA-approved T cell BsAb, blinatumomab (which uses L2K, a minor variant) (23).

The comparison of BsAbs in both syngeneic and xenograft animal models also revealed important differences between the various formats. It is tempting to speculate that among the tested designs, only the IgG-[L]-scFv had the stimulatory power to elicit productive in vivo responses from naïve T cells, which are more difficult to activate than effector T cells and take a longer time to respond. It is also notable that the capacity of each BsAb to elicit antigen-dependent IL-2 release from T cells in vitro was the best predictor of in vivo activity in all animal models. This strong correlation between in vivo potency and in vitro IL-2

production from naïve T cells highlights the importance of T cell cytokines as components of productive anti-tumor responses in addition to being biomarkers of T cell activation. Although recent work (24) has suggested that anti-leukemia activity may not require strong cytokine release, our data suggested that robust responses against solid tumors required potent IL-2 secretion. In light of these results, it may be worth re-evaluating design strategies aimed at minimizing cytokine production to mitigate side effects (25), because these same strategies might compromise clinical anti-tumor efficacy.

Prior studies have demonstrated that BsAb targeting epitopes close to the tumor cell membrane (proximal) elicited more potent T cell cytotoxicity than those that bound epitopes farther away (distal) (26, 27), implying that close apposition between T cells and tumor cells drives more effective T cell activation and killing. This phenomenon has been linked to the exclusion of the inhibitory phosphatase CD45 (27), which contains a large extracellular domain that cannot fit into tight intercellular spaces. Although this could explain why the cis-configured 1+1C performs better than the trans-configured 1+1T in our hands, the superiority of the 2+2 (IgG-[L]-scFv) format over the 2+2B (BiTE-Fc) design indicates that minimizing the distance between tumor antigen and T cell binding domains does not always improve BsAb performance. In that regard, it is important to note that the TCR is a mechanosensitive protein that undergoes activating conformational changes in response to forces applied to its ligand-binding domain (28, 29). Hence, the interdomain spacing imparted by a C_L domain in the IgG-[L]-scFv format may provide the most optimal physical constraint or mechanical coupling between the TCR and tumor cell, resulting in stronger and/or more sustained delivery of activating signals. Comparing the capacity of different BsAb formats to induce TCR conformational change will be an interesting topic for future work.

Our study also strongly supports the feasibility of developing BsAbs with bivalency towards T cells. Although many BsAb designs currently in clinical development use tumor bivalency to increase potency (22, 30) or to improve selectivity (31), bivalency against T cell epitopes has largely been avoided for fear of non-specific activation (32). We found, however, that the additional cis-module generated by adding a second anti-CD3 scFv to 2+1 dramatically improved both in vitro and in vivo functionality (compare 2+1 to 2+2) without inducing toxicity. Interestingly, although 2+2 did show superior T cell binding compared to 2+1, it was inferior to both 2+2B and 2+2HC, which also contained two anti-CD3 scFv domains. We can only speculate as to why 2+2 binds T cells less strongly than the other bivalent BsAbs. It may be that the IgG-[L]-scFv format imparts structural constraints, not present in the 2+2B or the 2+2HC designs, that impede consistent bivalent T cell engagement. What is clear from our results, however, is that 2+2 outperformed both 2+2B and 2+2HC in anti-tumor function. Hence, T cell bivalency, when combined with the proper interdomain spacing and spatial configuration, can afford critical improvements in activity that are independent of its capacity to enhance T cell binding. Lastly, as a dual bivalent design, the IgG-[L]-scFv format gains the added benefit of being symmetrical and is therefore less complicated to manufacture relative to asymmetrical designs that combine tumor bivalency with T cell monovalency.

It is also important to note that monovalent T cell engagement does not necessarily eliminate clinical toxicities such as cytokine release or antigen-independent immune activation. Many dual monovalent formats such as blinatumomab, the FDA-approved anti-CD19 BiTE, or tandem-scFv BsAb targeting CD123, induced substantial cytokine release or neurotoxicity during their clinical development (33–37), although this has been ameliorated by the use of tocilizumab and pre-treatment with steroids (38). Although the added complexity of extra binding domains might be expected to complicate clinical grade development (by compromising stability or reagent purity) or increase immunogenicity, relative to monovalent designs, we have not observed these issues when generating clinical scale quantities of the anti-GD2 IgG-[L]-scFv BsAb. A phase I clinical trial of the GD2-specific 2+2 is currently underway (NCT03870207), and it will be interesting to compare any immune-mediated side effects with those that have been reported for monovalent BsAb.

Despite 30 years of development to date, only one T cell BsAb has been clinically approved by the FDA, with most failing due to insufficient potency in the face of dose-limiting toxicities (typically cytokine release-related). Here, we have shown that cis-configured binding domains and dual bivalency can provide log-fold improvements to T cell BsAb potencies in vitro and superior efficacies in vivo. If incorporated into future BsAb design strategies, these conceptual guidelines may substantially improve clinical outcomes. While the IgG-[L]-scFv design may not be optimal for all anti-CD3 sequences, or against certain classes of tumor antigens (large bulky proteins, secreted or cleaved epitopes, etc.) we believe it represents a good standard for most T cell engaging BsAbs and is a marked improvement over many other conventional formats. By combining the benefits of symmetry (2+2), spatial configuration (cis), interdomain spacing (C_L), and pharmacokinetics (IgG-like), an OKT3-based IgG-[L]-scFv could potentially drive forward both clinical progress and academic studies in coming years.

Materials and Methods

Study design

The primary objective of this study was to identify the effects of BsAb format on in vitro and in vivo anti-tumor function. We compared nine BsAb formats using human and murine T cells, cell lines, and human PDX tumors.

For in vivo experiments, sample sizes were determined based on the observed variation in tumor progression and response in previous studies (9, 12, 13). Four to five animals were used for each group in every animal experiment. Mice were followed until tumors became too large (>1,500 mm^3), and no data were excluded. All mice from the same treatment groups were co-housed in the same cage. Experiments using female mice were completely randomized after tumor implantation, but before their initial treatment. Experiments using male mice had cages randomized after tumor implantation and before the start of treatment. Blinding of treatment or experimental measurements was not performed.

Animal studies

All experiments were performed in compliance with all relevant ethical regulations and in accordance with an Institutional Animal Care and Use Committee-approved protocol (protocol 09–05-010). All mice used in treatment studies were bred in the MSKCC animal facility. Mice for pharmacokinetic analysis were purchased. Weights and tumor volumes were measured once per week, and overall mouse health was evaluated at least three times per week. Tumor volumes were calculated using a TM900 measurement device (Peira) or caliper. For caliper measurements, volume measurements were estimated as [(L) x (W) x (W) x 0.5], where L is the longest diameter of the tumor, and W is the diameter perpendicular to L. Mice were sacrificed once tumor volumes reached 1.5–2.0 cm^3. No treatment-related toxicities (weight loss, hair loss, weakness, etc.) were observed in any mice throughout these experiments.

Three mouse models were used: 1) an immunodeficient xenograft model (12), 2) an immunodeficient “armed” T cell xenograft model (21), and 3) an immunocompetent huCD3ε-transgenic syngeneic model (19).

In the first model, 8- to 16-week-old male BALB/c IL-2rg$^{-/-}$, Rag2$^{-/-}$ (DKO, Taconic, 11503) mice were implanted subcutaneously with M14 melanoma cells or IMR32 neuroblastoma cells. After 5–15 days (tumors approximately 100–200 mm^3), mice were treated intravenously with huATC (40 or 20 million cells, once or twice per week, respectively), intravenously with BsAb (10–25 pmol, twice per week), and subcutaneously with human IL-2 (aldesleukin, 1,000 U, twice per week) for three weeks.

For the second model, 10- to 16-week-old male or female DKO mice were implanted with digested PDX tumors (each tumor was passaged into 10 new mice). Treatment began 8–20 days after implantation. For each treatment, huATCs were incubated in vitro with each BsAb for 20 minutes at room temperature. After the incubation, cells were washed once and injected intravenously into xenografted mice (20 million cells, twice per week) along with subcutaneous IL-2 (aldesleukin, 1,000 U, twice per week) for three weeks.

For the third model, B6.Cg-Tg(CD3E)600Cpt/J (huCD3ε-tg, Jackson Laboratory, 020456) mice were bred with wildtype C57BL/6 mice (Jackson Laboratory, 000664) to generate huCD3ε-tg F1 heterozygotes, which were used for all experiments. From here, 8- to 16-week-old male mice were implanted subcutaneously with 50,000 EL.4 lymphoma cells. After seven days, mice were treated intravenously with BsAb (25 pmol, twice per week) for three weeks. The BiTE was dosed daily (7 pmol per dose) for three weeks to account for poorer pharmacokinetics.

All cell line implantations used Matrigel (Corning, 354234) at a ratio of 3:1 by volume (Matrigel to cells). PDX tumors were implanted by the anti-tumor assessment core facility at MSKCC. Plasma was collected retroorbitally and stored at −80°C until assayed. CBC measurements were done on freshly collected whole blood (EDTA-neutralized) using an a HT5 Hematology Analyzer (Heska) in the anti-tumor assessment core facility. Data was plotted using GraphPad Prism 8.

Pharmacokinetic analysis

Female Balb/c nude mice (Envigo, 069(nu)/070(nu/+)) were injected with 100 μg of BsAb or mAb and bled serially over 7 days (30 minutes – 168 hours). Blood was processed as serum and frozen until all samples were acquired. Serum concentrations of BsAb or mAb were determined by ELISA. Briefly, wells were coated with anti-3F8 idiotype antibody (50 μl, 20 μg/ml) overnight at room temperature. After this, plates were washed with PBS and blocked with PBS supplemented with 0.5% bovine serum albumin (Sigma, A7906) for one hour at room temperature. Serum samples were added at 1:100 and 1:1,000 dilutions in duplicate and incubated at 37 °C for 2.5 hours. Samples were then detected with a mouse anti-human Fc specific secondary antibody conjugated with horseradish peroxidase (Southern Biotech, Clone 4E3, 9052–05) for one hour at 4 °C. Plates were developed with o-phenylenediamine (Sigma, P8287–100TAB) and stopped with 5 N sulfuric acid. Plates were read at 490 nm using a Biotek H1 plate reader (Synergy) with the Gen5 software (version v2.09). Protein concentrations were calculated using a standard curve of either 2+2 or hu3F8 IgG, fitted using a three-parameter logistic fitting. Pharmacokinetic analysis was carried out by non-compartmental analysis of the serum concentration-time data using WinNonlin software program (Pharsight Corp.).

Statistical analyses

All statistical analyses were performed using Prism software version 8.0 (GraphPad). P values for comparisons between multiple groups were determined by two-way analysis of variance (ANOVA) with subsequent Tukey correction. For all statistical tests, a P value of <0.05 was used to denote statistical significance. All error bars denote the standard deviation, unless otherwise noted in the figure legends. Original data are in data file S1.

Supplementary Material

Refer to Web version on PubMed Central for supplementary material.

Acknowledgments:

We thank Dr. Mamoru Ito of Central Institute for Experimental Animals, Kawasaki, Japan, for providing the DKO mice, and Dr. Sampson of Duke University, Durham North Carolina, for providing the huCD3ε-tg mice. We also thank Dr. Elisa de Stanchina for her help in developing and passaging the patient-derived xenograft tumors.

Funding: This work was supported by funds from Enid A. Haupt Endowed Chair (to N.-K.V.C.), the Robert Steel Foundation (to N.-K.V.C.), the Grayer Fellowship (to B.H.S.), and the NIH/NCI Cancer Center Support Grant P30 CA008748.

References and Notes:

1. Shima M, Hanabusa H, Taki M, Matsushita T, Sato T, Fukutake K, Fukazawa N, Yoneyama K, Yoshida H, Nogami K, Factor VIII-Mimetic Function of Humanized Bispecific Antibody in Hemophilia A. N Engl J Med 374, 2044–2053 (2016). [PubMed: 27223146]
2. Topp MS, Gokbuget N, Stein AS, Zugmaier G, O'Brien S, Bargou RC, Dombret H, Fielding AK, Heffner L, Larson RA, Neumann S, Foa R, Litzow M, Ribera JM, Rambaldi A, Schiller G, Bruggemann M, Horst HA, Holland C, Jia C, Maniar T, Huber B, Nagorsen D, Forman SJ, Kantarjian HM, Safety and activity of blinatumomab for adult patients with relapsed or refractory B-precursor acute lymphoblastic leukaemia: a multicentre, single-arm, phase 2 study. Lancet Oncol 16, 57–66 (2015). [PubMed: 25524800]

3. Ishiguro T, Sano Y, Komatsu SI, Kamata-Sakurai M, Kaneko A, Kinoshita Y, Shiraiwa H, Azuma Y, Tsunenari T, Kayukawa Y, Sonobe Y, Ono N, Sakata K, Fujii T, Miyazaki Y, Noguchi M, Endo M, Harada A, Frings W, Fujii E, Nanba E, Narita A, Sakamoto A, Wakabayashi T, Konishi H, Segawa H, Igawa T, Tsushima T, Mutoh H, Nishito Y, Takahashi M, Stewart L, ElGabry E, Kawabe Y, Ishigai M, Chiba S, Aoki M, Hattori K, Nezu J, An anti-glypican 3/CD3 bispecific T cell-redirecting antibody for treatment of solid tumors. Sci Transl Med 9, eaal4291 (2017).
4. Cheal SM, Xu H, Guo HF, Zanzonico PB, Larson SM, Cheung NK, Preclinical evaluation of multistep targeting of diasialoganglioside GD2 using an IgG-scFv bispecific antibody with high affinity for GD2 and DOTA metal complex. Mol Cancer Ther 13, 1803–1812 (2014). [PubMed: 24944121]
5. Brinkmann U, Kontermann RE, The making of bispecific antibodies. MAbs 9, 182–212 (2017). [PubMed: 28071970]
6. Spiess C, Zhai Q, Carter PJ, Alternative molecular formats and therapeutic applications for bispecific antibodies. Mol Immunol 67, 95–106 (2015). [PubMed: 25637431]
7. Wu Z, Cheung NV, T cell engaging bispecific antibody (T-BsAb): From technology to therapeutics. Pharmacol Ther 182, 161–175 (2018). [PubMed: 28834699]
8. Cuesta AM, Sainz-Pastor N, Bonet J, Oliva B, Alvarez-Vallina L, Multivalent antibodies: when design surpasses evolution. Trends Biotechnol 28, 355–362 (2010). [PubMed: 20447706]
9. Cheng M, Santich BH, Xu H, Ahmed M, Huse M, Cheung NK, Successful engineering of a highly potent single-chain variable-fragment (scFv) bispecific antibody to target disialoganglioside (GD2) positive tumors. Oncoimmunology 5, e1168557 (2016).
10. Hoseini SS, Guo H, Wu Z, Hatano MN, Cheung NV, A potent tetravalent T-cell-engaging bispecific antibody against CD33 in acute myeloid leukemia. Blood Adv 2, 1250–1258 (2018). [PubMed: 29858209]
11. Wu Z, Guo HF, Xu H, Cheung NV, Development of a Tetravalent Anti-GPA33/Anti-CD3 Bispecific Antibody for Colorectal Cancers. Mol Cancer Ther 17, 2164–2175 (2018). [PubMed: 30082472]
12. Lopez-Albaitero A, Xu H, Guo H, Wang L, Wu Z, Tran H, Chandarlapaty S, Scaltriti M, Janjigian Y, de Stanchina E, Cheung NK, Overcoming resistance to HER2-targeted therapy with a novel HER2/CD3 bispecific antibody. Oncoimmunology 6, e1267891 (2017).
13. Xu H, Cheng M, Guo H, Chen Y, Huse M, Cheung NK, Retargeting T cells to GD2 pentasaccharide on human tumors using Bispecific humanized antibody. Cancer Immunol Res 3, 266–277 (2015). [PubMed: 25542634]
14. Cheung NK, Guo H, Hu J, Tassev DV, Cheung IY, Humanizing murine IgG3 anti-GD2 antibody m3F8 substantially improves antibody-dependent cell-mediated cytotoxicity while retaining targeting in vivo. Oncoimmunology 1, 477–486 (2012). [PubMed: 22754766]
15. Adair JR, Athwal DS, Bodmer MW, Bright SM, Collins AM, Pulito VL, Rao PE, Reedman R, Rothermel AL, Xu D, et al., Humanization of the murine anti-human CD3 monoclonal antibody OKT3. Hum Antibodies Hybridomas 5, 41–47 (1994). [PubMed: 7858182]
16. Labrijn AF, Meesters JI, Priem P, de Jong RN, van den Bremer ET, van Kampen MD, Gerritsen AF, Schuurman J, Parren PW, Controlled Fab-arm exchange for the generation of stable bispecific IgG1. Nat Protoc 9, 2450–2463 (2014). [PubMed: 25255089]
17. Leo O, Foo M, Sachs DH, Samelson LE, Bluestone JA, Identification of a monoclonal antibody specific for a murine T3 polypeptide. Proc Natl Acad Sci U S A 84, 1374–1378 (1987). [PubMed: 2950524]
18. Ahmed M, Cheng M, Cheung IY, Cheung NK, Human derived dimerization tag enhances tumor killing potency of a T-cell engaging bispecific antibody. Oncoimmunology 4, e989776 (2015).
19. Gedeon PC, Schaller TH, Chitneni SK, Choi BD, Kuan CT, Suryadevara CM, Snyder DJ, Schmittling RJ, Szafranski SE, Cui X, Healy PN, Herndon JE 2nd, McLendon RE, Keir ST, Archer GE, Reap EA, Sanchez-Perez L, Bigner DD, Sampson JH, A Rationally Designed Fully Human EGFRvIII:CD3-Targeted Bispecific Antibody Redirects Human T Cells to Treat Patient-derived Intracerebral Malignant Glioma. Clin Cancer Res 24, 3611–3631 (2018). [PubMed: 29703821]

20. Coloma MJ, Morrison SL, Design and production of novel tetravalent bispecific antibodies. Nat Biotechnol 15, 159–163 (1997). [PubMed: 9035142]
21. Yankelevich M, Kondadasula SV, Thakur A, Buck S, Cheung NK, Lum LG, Anti-CD3 x anti-GD2 bispecific antibody redirects T-cell cytolytic activity to neuroblastoma targets. Pediatr Blood Cancer 59, 1198–1205 (2012). [PubMed: 22707078]
22. Bacac M, Colombetti S, Herter S, Sam J, Perro M, Chen S, Bianchi R, Richard M, Schoenle A, Nicolini V, Diggelmann S, Limani F, Schlenker R, Husser T, Richter W, Bray-French K, Hinton H, Giusti AM, Freimoser-Grundschober A, Lariviere L, Neumann C, Klein C, Umana P, CD20-TCB with Obinutuzumab Pretreatment as Next-Generation Treatment of Hematologic Malignancies. Clin Cancer Res 24, 4785–4797 (2018). [PubMed: 29716920]
23. Dreier T, Lorenczewski G, Brandl C, Hoffmann P, Syring U, Hanakam F, Kufer P, Riethmuller G, Bargou R, Baeuerle PA, Extremely potent, rapid and costimulation-independent cytotoxic T-cell response against lymphoma cells catalyzed by a single-chain bispecific antibody. Int J Cancer 100, 690–697 (2002). [PubMed: 12209608]
24. Trinklein ND, Pham D, Schellenberger U, Buelow B, Boudreau A, Choudhry P, Clarke SC, Dang K, Harris KE, Iyer S, Jorgensen B, Pratap PP, Rangaswamy US, Ugamraj HS, Vafa O, Wiita AP, van Schooten W, Buelow R, Force Aldred S, Efficient tumor killing and minimal cytokine release with novel T-cell agonist bispecific antibodies. MAbs 11, 639–652 (2019). [PubMed: 30698484]
25. Ellerman D, Bispecific T-cell engagers: Towards understanding variables influencing the in vitro potency and tumor selectivity and their modulation to enhance their efficacy and safety. Methods 154, 102–117 (2019). [PubMed: 30395966]
26. Bluemel C, Hausmann S, Fluhr P, Sriskandarajah M, Stallcup WB, Baeuerle PA, Kufer P, Epitope distance to the target cell membrane and antigen size determine the potency of T cell-mediated lysis by BiTE antibodies specific for a large melanoma surface antigen. Cancer Immunol Immunother 59, 1197–1209 (2010). [PubMed: 20309546]
27. Li J, Stagg NJ, Johnston J, Harris MJ, Menzies SA, DiCara D, Clark V, Hristopoulos M, Cook R, Slaga D, Nakamura R, McCarty L, Sukumaran S, Luis E, Ye Z, Wu TD, Sumiyoshi T, Danilenko D, Lee GY, Totpal K, Ellerman D, Hotzel I, James JR, Junttila TT, Membrane-Proximal Epitope Facilitates Efficient T Cell Synapse Formation by Anti-FcRH5/CD3 and Is a Requirement for Myeloma Cell Killing. Cancer Cell 31, 383–395 (2017). [PubMed: 28262555]
28. Liu B, Chen W, Evavold BD, Zhu C, Accumulation of dynamic catch bonds between TCR and agonist peptide-MHC triggers T cell signaling. Cell 157, 357–368 (2014). [PubMed: 24725404]
29. Kim ST, Takeuchi K, Sun ZY, Touma M, Castro CE, Fahmy A, Lang MJ, Wagner G, Reinherz EL, The alphabeta T cell receptor is an anisotropic mechanosensor. J Biol Chem 284, 31028–31037 (2009). [PubMed: 19755427]
30. Bacac M, Klein C, Umana P, CEA TCB: A novel head-to-tail 2:1 T cell bispecific antibody for treatment of CEA-positive solid tumors. Oncoimmunology 5, e1203498 (2016).
31. Slaga D, Ellerman D, Lombana TN, Vij R, Li J, Hristopoulos M, Clark R, Johnston J, Shelton A, Mai E, Gadkar K, Lo AA, Koerber JT, Totpal K, Prell R, Lee G, Spiess C, Junttila TT, Avidity-based binding to HER2 results in selective killing of HER2-overexpressing cells by anti-HER2/CD3. Sci Transl Med 10, 5775 (2018).
32. Moore GL, Bautista C, Pong E, Nguyen DH, Jacinto J, Eivazi A, Muchhal US, Karki S, Chu SY, Lazar GA, A novel bispecific antibody format enables simultaneous bivalent and monovalent co-engagement of distinct target antigens. MAbs 3, 546–557 (2011). [PubMed: 22123055]
33. Klinger M, Brandl C, Zugmaier G, Hijazi Y, Bargou RC, Topp MS, Gokbuget N, Neumann S, Goebeler M, Viardot A, Stelljes M, Bruggemann M, Hoelzer D, Degenhard E, Nagorsen D, Baeuerle PA, Wolf A, Kufer P, Immunopharmacologic response of patients with B-lineage acute lymphoblastic leukemia to continuous infusion of T cell-engaging CD19/CD3-bispecific BiTE antibody blinatumomab. Blood 119, 6226–6233 (2012). [PubMed: 22592608]
34. Ravandi F, Stein AS, Kantarjian HM, Walter RB, Paschka P, Jongen-Lavrencic M, Ossenkoppele GJ, Yang Z, Mehta B, Subklewe M, A Phase 1 First-in-Human Study of AMG 330, an Anti-CD33 Bispecific T-Cell Engager (BiTE (R)) Antibody Construct, in Relapsed/Refractory Acute Myeloid Leukemia (R/R AML). Blood 132, (2018).
35. Hutchings M, Iacoboni G, Morschhauser F, Offner F, Sureda A, Salles GA, Carlo-Stella C, Lopez JM, Thomas D, Morcos PN, Quackenbush B, Ferlini C, Bacac M, Broeske AME, Dimier N,

Moore T, Weisser M, Dickinson M, CD20-Tcb (RG6026), a Novel “ 2:1 “ Format T-Cell-Engaging Bispecific Antibody, Induces Complete Remissions in Relapsed/Refractory B-Cell Non-Hodgkin’s Lymphoma: Preliminary Results from a Phase I First in Human Trial. Blood 132, (2018).

36. Uy GL, Godwin J, Rettig MP, Vey N, Foster M, Arellano ML, Rizzieri DA, Topp MS, Huls G, Lowenberg B, Martinelli G, Paolini S, Ciceri F, Carrabba MG, Ballesteros-Merino C, Bifulco CB, Lelievre H, La Motte-Mohs R, Li D, Sun JC, Jacobs K, Spohn K, Lonsdale N, Tran K, Baughman J, Shannon M, Fox B, Bonvini E, Wigginton J, Davidson-Moncada J, DiPersio JF, Preliminary Results of a Phase 1 Study of Flotetuzumab, a CD123 x CD3 Bispecific Dart (R) Protein, in Patients with Relapsed/Refractory Acute Myeloid Leukemia and Myelodysplastic Syndrome. Blood 130, (2017).
37. Chichili GR, Huang L, Li H, Burke S, He L, Tang Q, Jin L, Gorlatov S, Ciccarone V, Chen F, Koenig S, Shannon M, Alderson R, Moore PA, Johnson S, Bonvini E, A CD3xCD123 bispecific DART for redirecting host T cells to myelogenous leukemia: preclinical activity and safety in nonhuman primates. Sci Transl Med 7, 289ra282 (2015).
38. Friberg G, Reese D, Blinatumomab (Blincyto): lessons learned from the bispecific t-cell engager (BiTE) in acute lymphocytic leukemia (ALL). Ann Oncol 28, 2009–2012 (2017). [PubMed: 28379283]

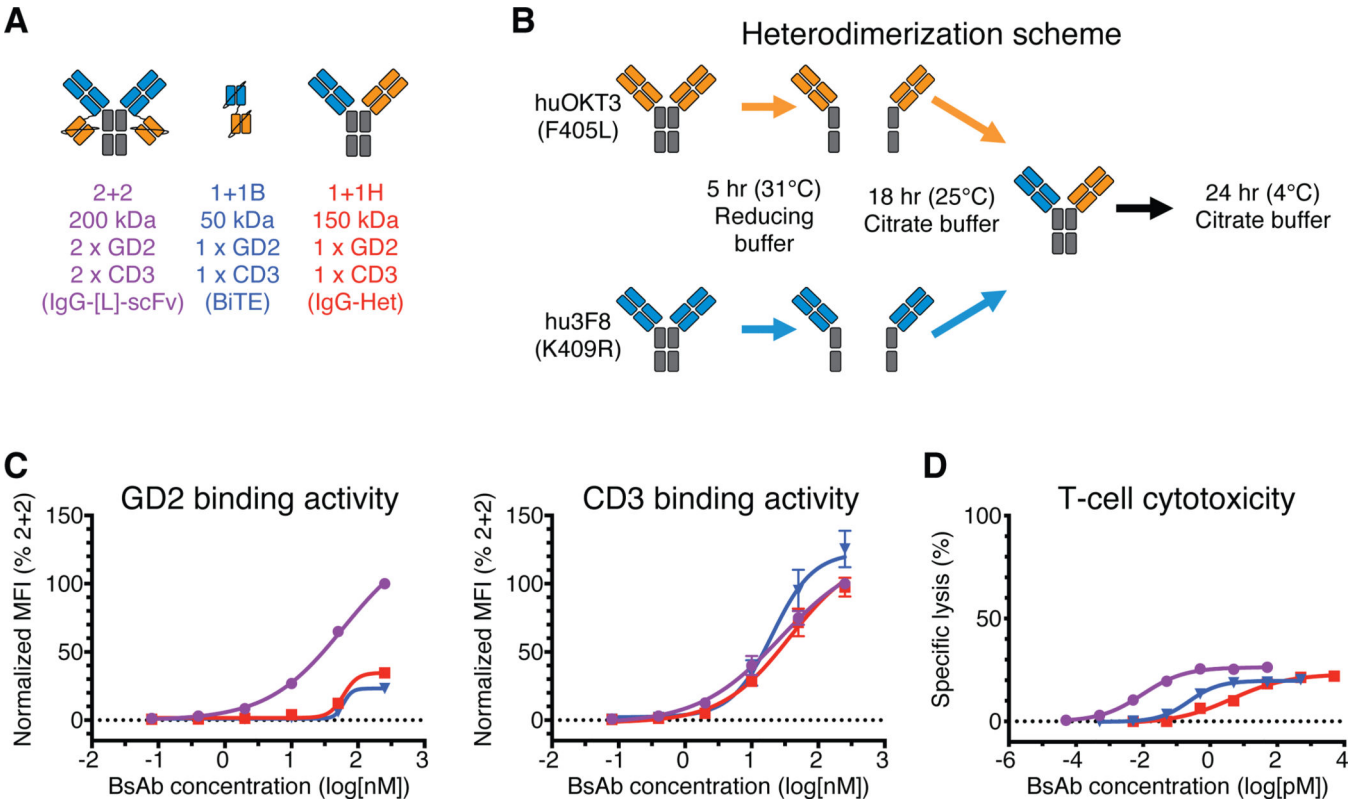

Fig. 1.

In vitro comparison of IgG-[L]-scFv to common BsAb designs

(A) Schematic of BsAb panel: IgG-[L]-scFv (2+2), BiTE (1+1B), and IgG-heterodimer (1+1H). Orange domains represent anti-huCD3ε domains (derived from huOKT3) and blue domains represent anti-GD2 domains (derived from hu3F8). (B) Schematic of the IgG heterodimerization by controlled Fab Arm Exchange. (C) Representative cell-binding activity of each BsAb against GD2(+) human M14 melanoma cells (left) and CD3(+) activated human T cells (right), measured by flow cytometry. Geometric mean intensity was normalized to 2+2 (100%) for each BsAb. (D) Representative T cell-dependent cytotoxicity for each BsAb. For reference: 2+2 is purple, 1+1B is blue, and 1+1H is red. Each curve represents one BsAb, and each point represents a single concentration, with two (FACS) or three (cytotoxicity) technical replicates. Data are shown as means ± standard deviation.

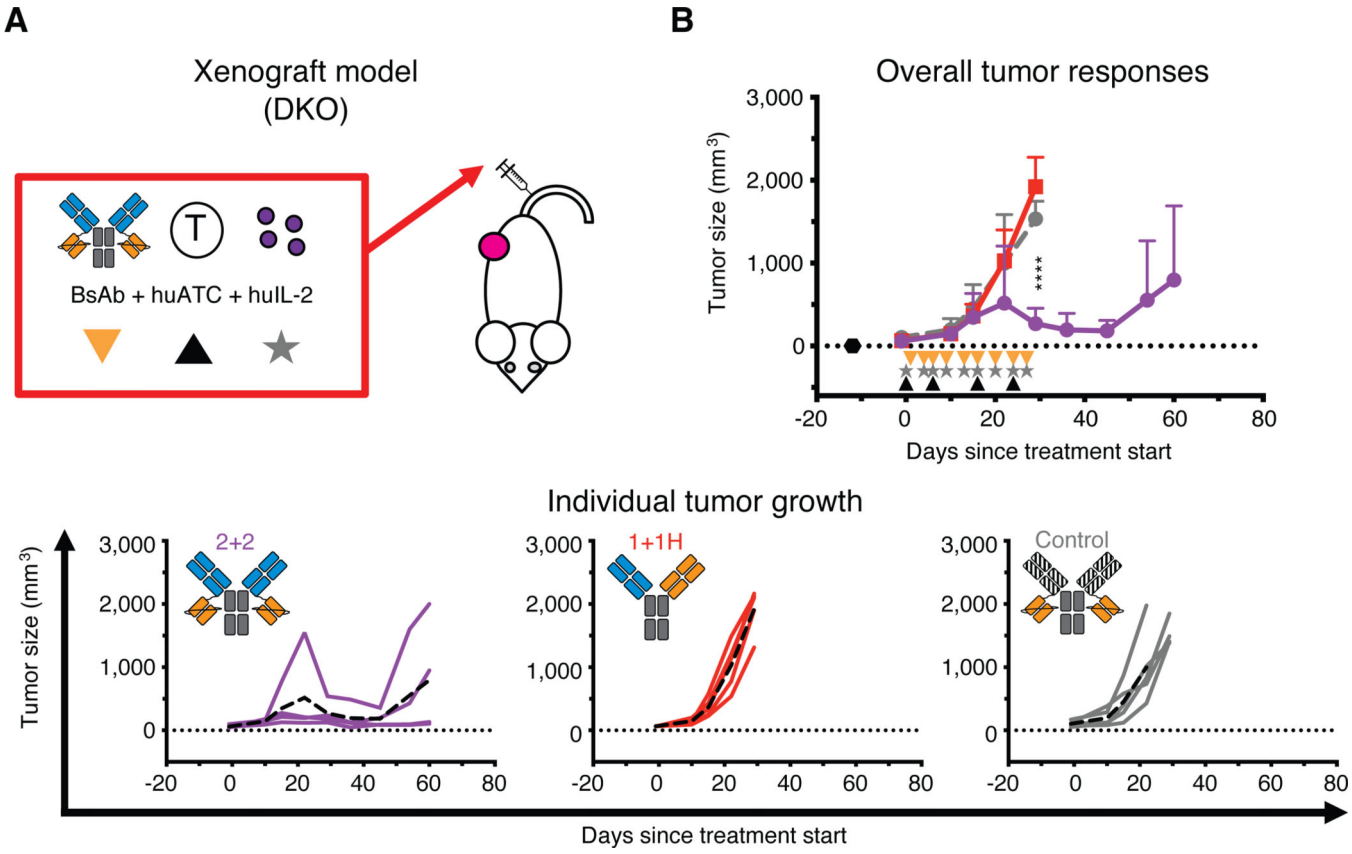

Fig. 2.

In vivo comparison of IgG-[L]-scFv to common BsAb designs

(A) Schematic of the treatment design for the xenograft tumor model. 25 pmol of BsAb was administered intravenously twice per week (black triangle), 40 million activated human T cells (huATC) were administered intravenously once per week (orange triangle), and human IL-2 (1,000 U) was administered subcutaneously twice per week (gray star). An anti-GPA33 BsAb was used as a control. (B) Average (top) and individual mouse (bottom) tumor responses in each group. In the overall response graph, each line represents one treatment group (n=4–5). The dotted black line represents no measurable tumor, and the black hexagon represents the tumor implantation. Tumor averages were calculated until at least one mouse had to be euthanized. Data are shown as means ± standard deviation. In the individual response graphs, each line represents a single mouse, and the dashed line represents the group average. For reference: 2+2 is purple, 1+1H is red, and the control BsAb is gray. Statistical significances were calculated by two-way analysis of variance (ANOVA) with Tukey correction. ****P < 0.0001 for control or 1+1H compared to 2+2.

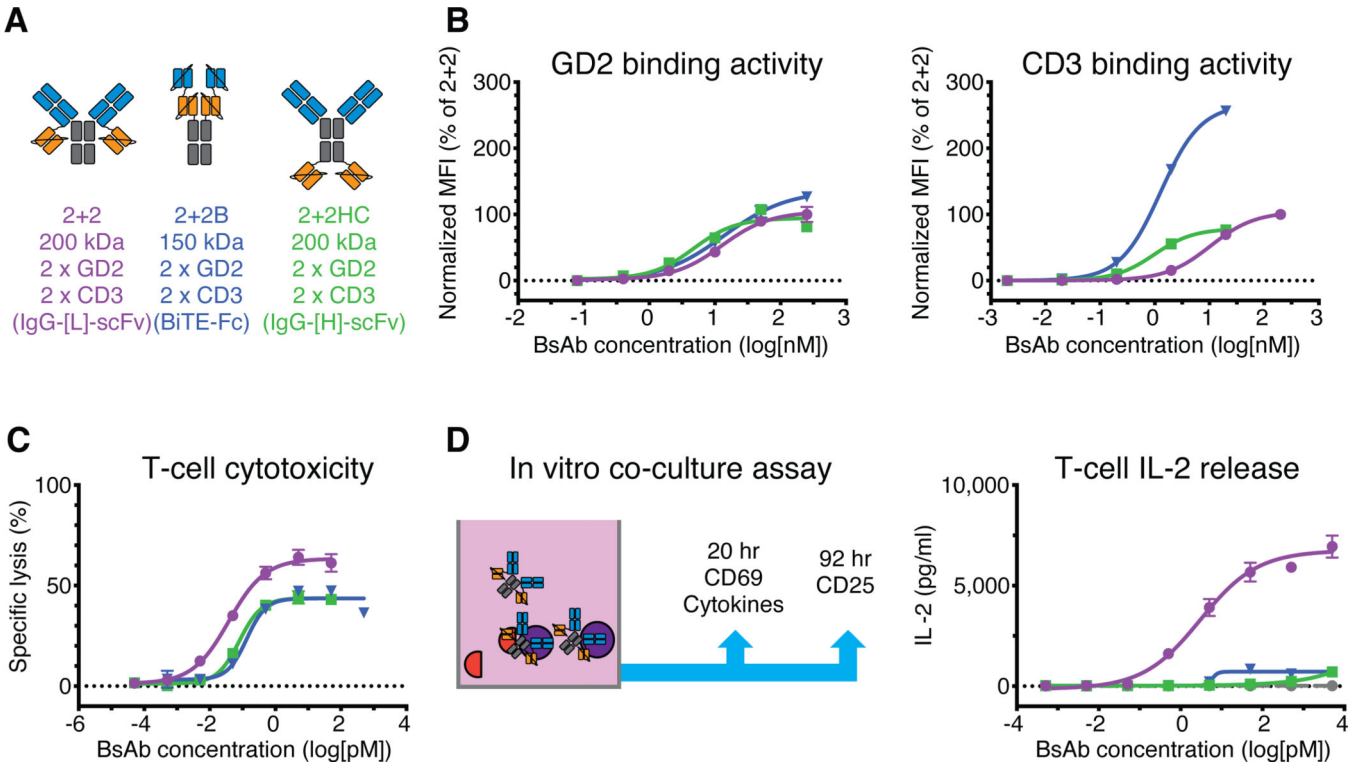

Fig. 3.

Comparison of dual bivalent BsAb designs

(A) Schematic of dual bivalent BsAb panel: IgG-[L]-scFv (2+2), BiTE-Fc (2+2B), and IgG-[H]-scFv (2+2HC). Orange represents anti-huCD3ε domains (derived from huOKT3) and blue represents anti-GD2 domains (derived from hu3F8). (B) Representative cell-binding activity of each BsAb against GD2(+) human M14 melanoma cells (left) and CD3(+) activated human T cells (right), measured by flow cytometry. Geometric mean intensity was normalized to 2+2 (100%) for each BsAb. (C) Representative T cell-dependent cytotoxicity for each BsAb. (D) Schematic of in vitro co-culture assay (left) and graph of results (right). For reference: 2+2 is purple, 2+2B is blue, and 2+2HC is green. Each curve represents one BsAb, and each point represents a single concentration, with two (FACS, cytokine) or three (cytotoxicity) technical replicates. Data are shown as means ± standard deviation.

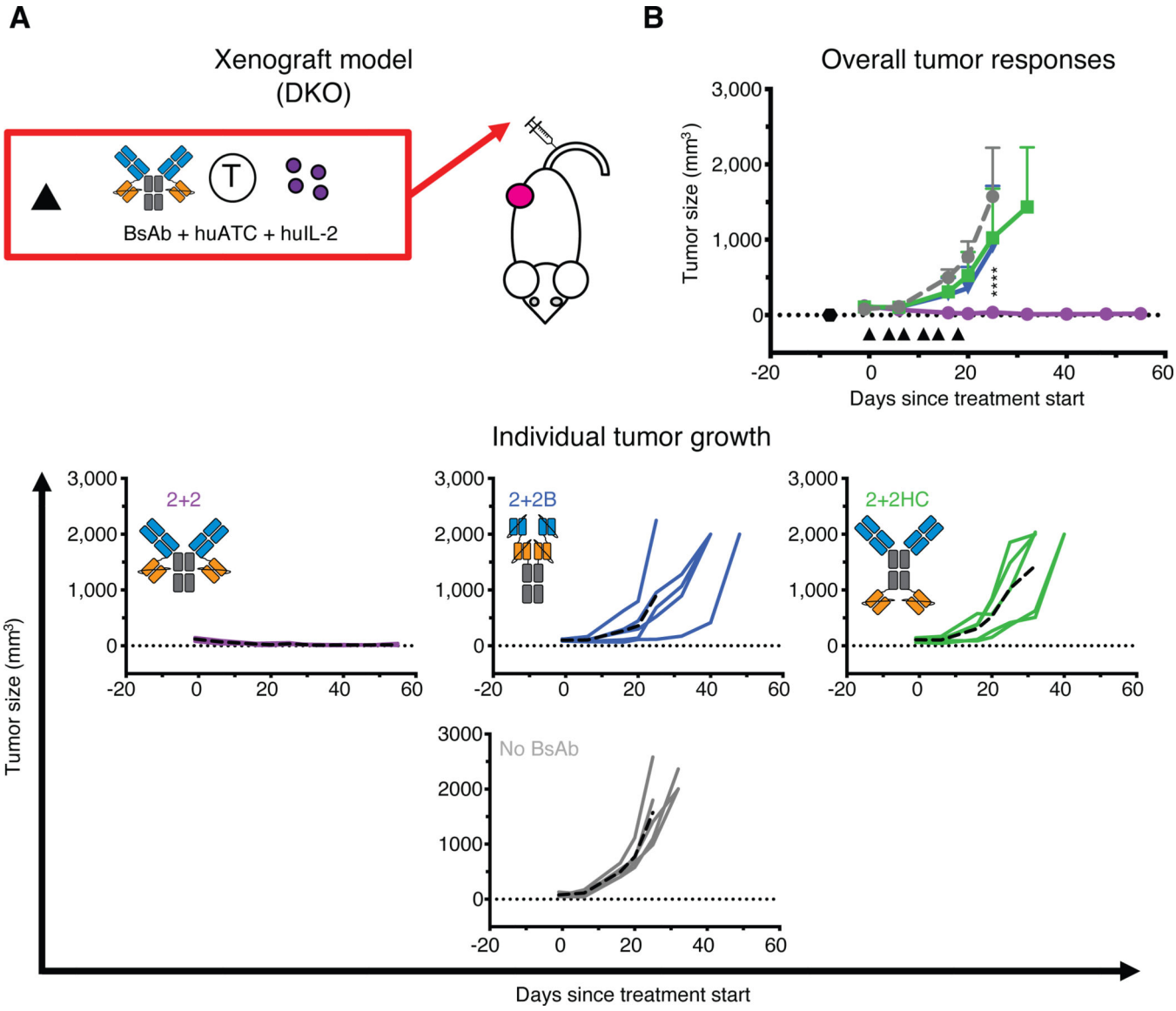

Fig. 4.

In vivo tumor responses of dual bivalent BsAb designs

(A) Schematic of the treatment design for the xenograft tumor model. 10 pmol of BsAb was administered intravenously twice per week along with 20 million activated human T cells (huATC) and subcutaneous human IL-2 (1,000 U) (black triangle). (B) Average (top) and individual mouse (bottom) tumor responses in each group. In the overall response graph, each line represents one treatment group (n=5). The dotted black line represents no measurable tumor, and the black hexagon represents the tumor implantation. Tumor averages were calculated until at least one mouse had to be euthanized. Data are shown as means ± standard deviation. In the individual response graphs, each line represents a single mouse, and the dashed line represents the group average. For reference: 2+2 is purple, 2+2B is blue, 2+2HC is green and the control group (no BsAb) is gray. Statistical significances

were calculated by two-way analysis of variance (ANOVA) with Tukey correction. ****P < 0.0001 for control, 2+2HC, or 2+2B compared to 2+2.

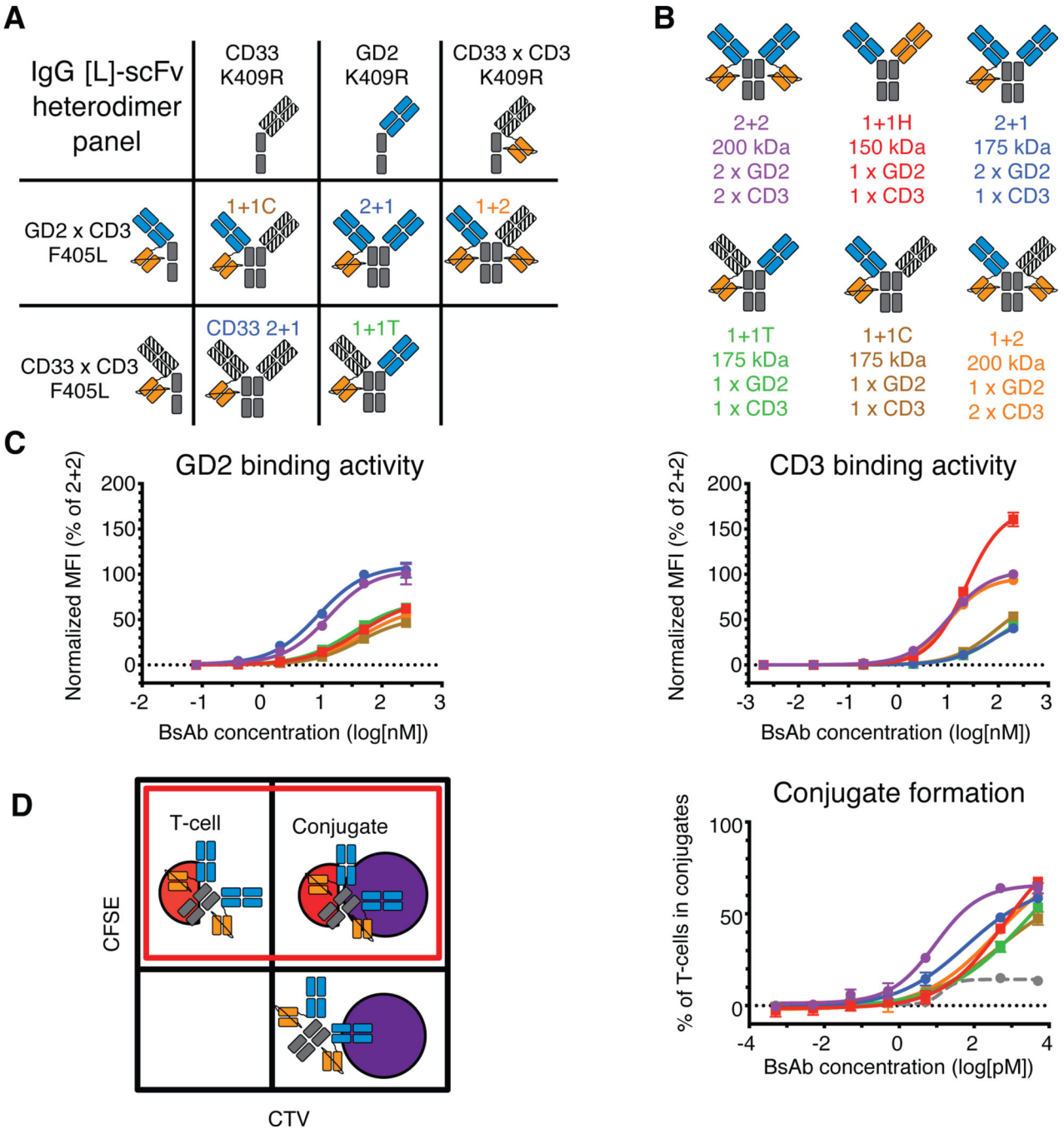

Fig. 5.

In vitro binding activity of IgG-[L]-scFv panel

(A) Schematic of heterodimerization strategy for the IgG-[L]-scFv panel. (B) Resulting IgG-[L]-scFv panel: 2+2, 1+1H, 2+1, 1+1T, 1+1C, and 1+2. Orange domains represent anti-huCD3ε domains (derived from huOKT3), blue domains represent anti-GD2 domains (derived from hu3F8), and striped black domains represent irrelevant anti-CD33 domain (derived from huM195). (C) Representative cell-binding activity of each BsAb against GD2(+) human M14 melanoma cells (left) and CD3(+) activated human T cells (right),

measured by flow cytometry. Geometric mean intensity was normalized to 2+2 (100%) for each BsAb. (D) Schematic of conjugate assay analysis (left) and graph of results (right). Unconjugated cells (upper left and lower right quadrants) displayed fluorescence under one channel, while conjugated cells (upper right quadrant) displayed fluorescence under two channels. For analysis, conjugate frequency was measured as the fraction of conjugated T cells among the total T cells (red box). An anti-CD33 BsAb was used as a control. Graphed values represent the amount of conjugate formation at each concentration of BsAb. For reference: 2+2 is purple, 1+1H is red, 2+1 is blue, 1+1T is green, 1+1C is brown, 1+2 is orange, and the control BsAb is gray. Each curve represents one BsAb, and each point represents a single concentration, with two technical replicates. Data are shown as means ± standard deviation.

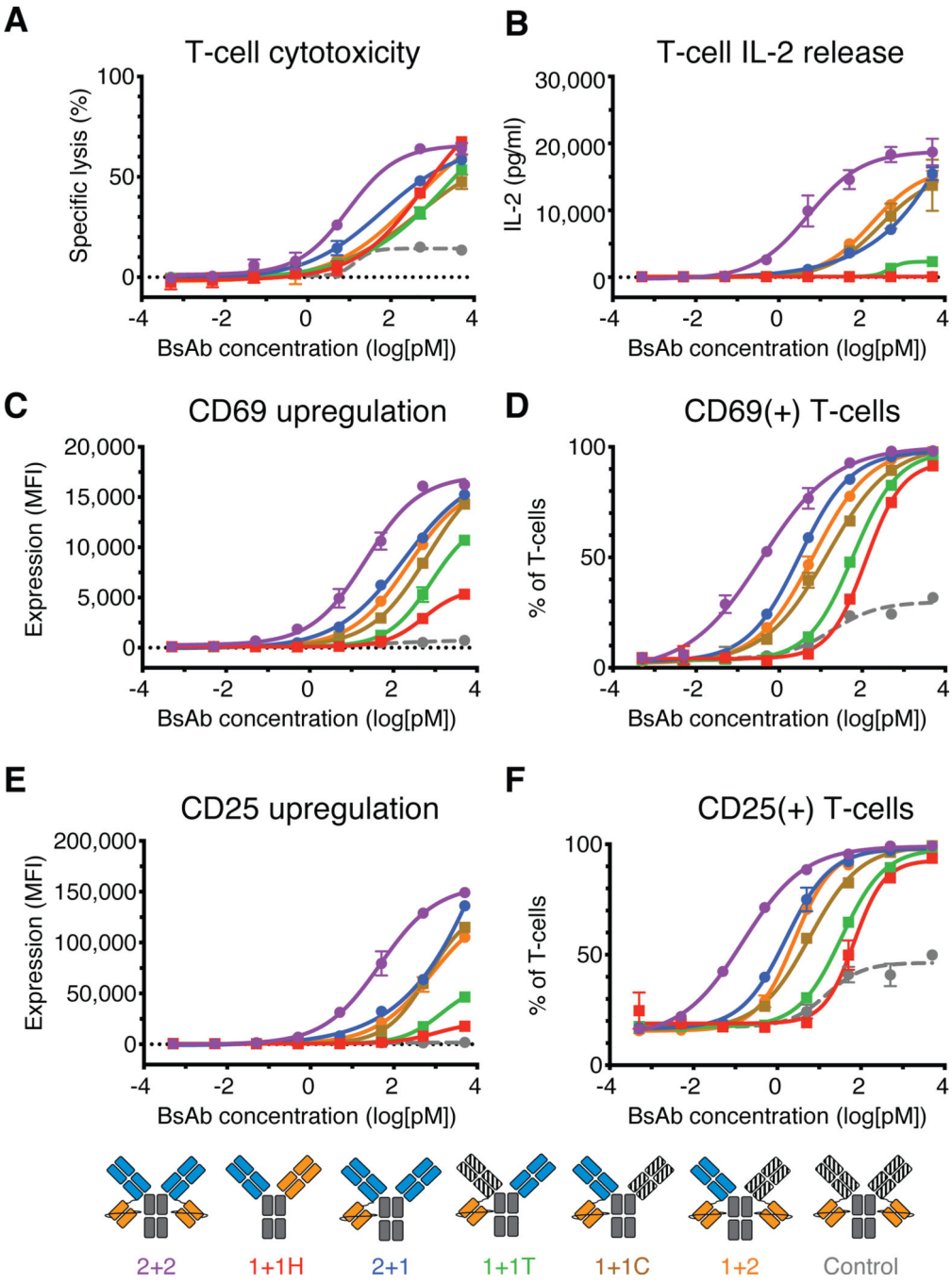

Fig. 6.

In vitro functional activity of IgG-[L]-scFv panel

(A) Representative T cell-dependent cytotoxicity of each BsAb. (B-E) T cell activation data from co-culture assays. (B) IL-2 cytokine release after 20 hours of co-culture. (C) CD69 expression intensity and (D) frequency of expression on T cells after 20 hours of co-culture. (E) CD25 expression intensity and (F) frequency of expression on T cells after 92 hours of co-culture. Assays included an anti-CD33 BsAb as a control. Schematic (bottom) for reference: 2+2 is purple, 1+1H is red, 2+1 is blue, 1+1T is green, 1+1C is brown, 1+2 is

orange, and the control BsAb is gray. Each curve represents one BsAb, and each point represents a single concentration, with two (cytokine) or three (cytotoxicity) technical replicates. Data are shown as means ± standard deviation.

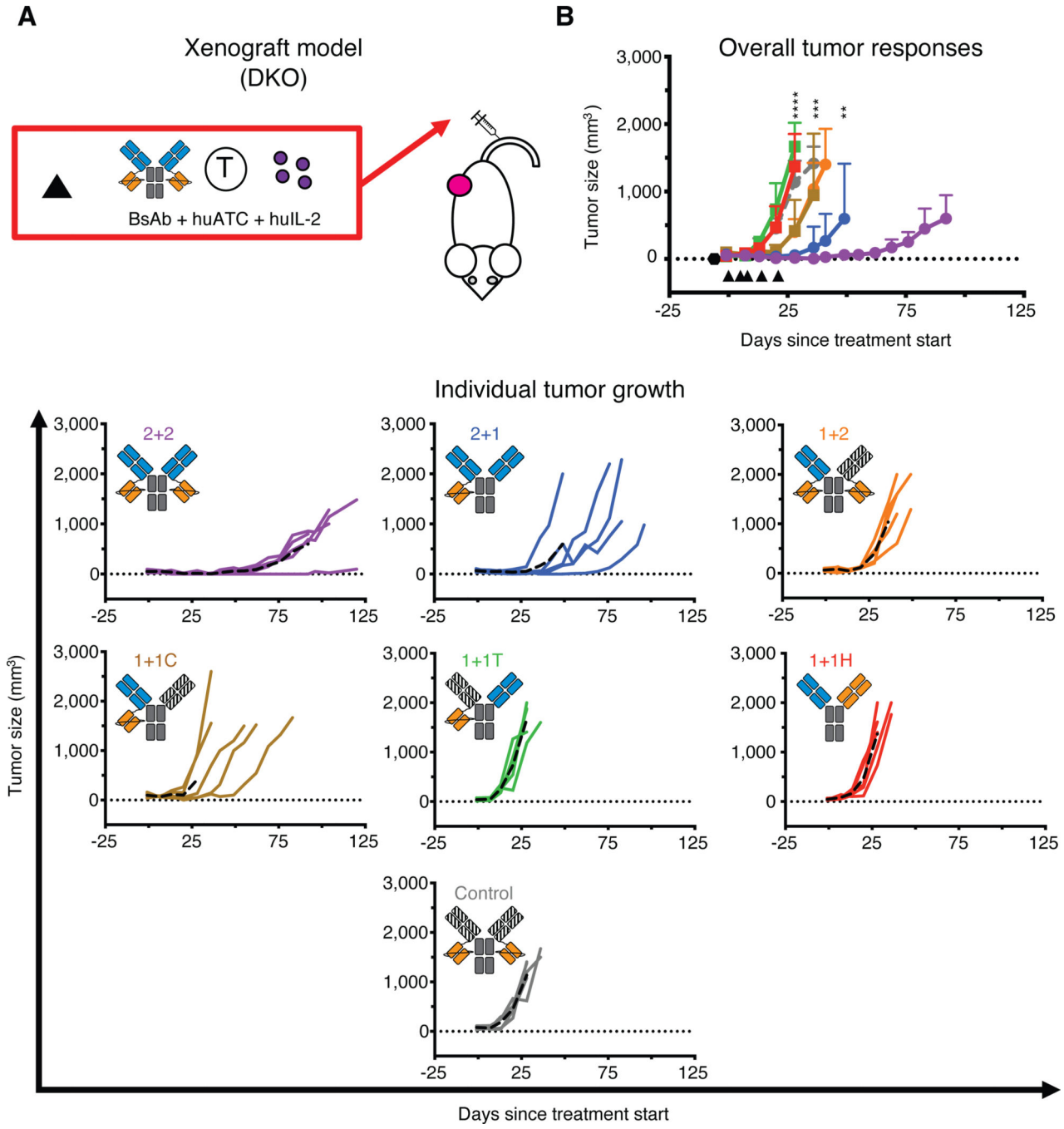

Fig. 7.

In vivo anti-tumor activity of IgG-[L]-scFv panel

Schematic of the treatment design for the xenograft tumor model. 25 pmol of BsAb was administered intravenously twice per week along with 20 million activated human T cells (huATC) and subcutaneous and human IL-2 (1,000 U) (black triangle). An anti-CD33 BsAb was used as a control. (B) Average (top) and individual mouse (bottom) tumor responses in each group. In the overall response graph, each line represents one treatment group (n=5). The dotted black line represents no measurable tumor, and the black hexagon represents the

tumor implantation. Tumor averages were calculated until at least one mouse had to be euthanized. Data are shown as means ± standard deviation. In the individual response graphs, each line represents a single mouse, and the dashed line represents the group average. For reference: 2+2 is purple, 1+1H is red, 2+1 is blue, 1+1T is green, 1+1C is brown, 1+2 is orange, and control BsAb is gray. Statistical significances were obtained by two-way analysis of variance (ANOVA) and Tukey correction. (C) ****$P < 0.0001$ for control, 1+1H, and 1+1T compared to 1+2, 1+1C, 2+1, or 2+2. ***$P < 0.001$ for 1+2 or 1+1C compared to 2+1 or 2+2. **$P < 0.01$ for 2+1 compared to 2+2.